Supporting Information

"Thermodynamic characterization of the multivalent interactions underlying rapid and selective translocation through the nuclear pore complex"

Ryo Hayama, Samuel Sparks, Lee M. Hecht, Kaushik Dutta, Jerome M. Karp, Christina M. Cabana, Michael P. Rout, David Cowburn

Table of Contents

Supplemental Methods

Protein Purifications

All FSFG construct-containing plasmids were transformed into BL21Gold(DE3) cells (Agilent, CA). Cells were grown in either LB or TB medium (12 g Tryptone, 24 g Yeast Extract, 4 ml glycerol, 2.31 g KH_2PO_4, and 12.54 g K_2HPO_4 per liter) with appropriate antibiotics at 37˚C to an OD_{600} of 0.6~0.8 and induced with 1 mM IPTG for 3 h at 37˚C at 250 rpm. Cells were harvested and stored at -80˚C. Cell pellets were resuspended in the FG-lysis buffer (20 mM HEPES-KOH (pH 7.4), 150 mM KCl, supplemented with cOmplete EDTA-free protease inhibitor tablet (Roche, NJ)) containing 8 M urea, lysed by microfluidizer, and centrifuged at 192,839 *g* for 1 h at 4˚C. The supernatant was collected and filtered through a 0.45 μm filter. The cleared lysate was passed through TALON resin (Clontech, CA) equilibrated with FG-Lysis Buffer containing 8 M urea to bind the protein. The column was washed with FG-lysis buffer with 8 M urea, FG-lysis buffer with 4 M urea, FG-lysis buffer with 10 mM imidazole, and the protein was eluted with elution buffer (20 mM HEPES-KOH, pH 6.8, 150 mM KCl, 250 mM imidazole). The fractions were analyzed by SDS-PAGE. The elution was concentrated by centrifugal concentrators with 3 kDa MWCO (EMD Millipore, MA), and dialyzed against Buffer A (20 mM HEPES-KOH, pH 6.8, 150 mM KCl, 2 mM $MgCl_2$) with 20% glycerol, frozen, and stored at -80˚C till use.

For sample containing [^{2}H, ^{15}N] NTF2, purification was performed in an identical manner as the unlabeled counterpart except that the purified sample was additionally dialyzed overnight into a high pH buffer containing 1 M urea (20 mM HEPES-KOH, pH 8, 150 mM KCl, 2 mM $MgCl_2$ 1 M urea) to exchange out the unobservable N^{2}H to N^{1}Hs. A subsequent dialysis was then performed exchange the buffer back to buffer A.

Isothermal Titration Calorimetry (ITC)

For each ITC experiment, concentrated stocks of $FSFG_x$ and NTF2 proteins were dialyzed against Buffer A twice at 4˚C. Samples were concentrated by Amicon Ultra-4 concentrators (EMD Millipore), centrifuged at 20,817*g* for 10 m, and filtered by COSTAR 0.45 μm centrifugal filters (Corning) to remove any large aggregates. The concentrations of the filtered proteins were measured by BCA assay. Concentrated, buffer matched samples, were diluted to desired concentrations with the dialysate (filtered and degassed).

Every experiment started with an injection of 0.4 µl NTF2, which was excluded from the subsequent analysis. Titrations were conducted in one of the three injection schemes: 19 injections of 2 µl, 10 injections of 2 µl followed by 6 injections of 3 µl, or 15 injections of 2.5 µl. The first scheme was typically employed for higher affinity FSFG construct, and the other two for lower affinity ones. Use of a two-volume injection scheme provides greater signal-to-noise in the latter half of the titration where the heat produced per mole of injectant diminishes (1).

Singular Value Decomposition (SVD) analysis

SVD analysis followed procedures described by Arai *et* al. (2). Briefly, the δ_H and δ_N from each HSQC spectra in the titration series involving [^{2}H-^{15}N]-NTF2 were represented as a one-dimensional column vector as $d = [\delta_{H1}, \ldots, \delta_{Hi}, \ldots, \delta_{Hm}, \delta_{N1}, \ldots, \delta_{Ni}, \ldots, \delta_{Nm}]$, where m is the number of assigned residues within NTF2 and i is the residue number. The HSQC spectra obtained within a series with n titrations points can be represented as a $2m$ X n data matrix $\boldsymbol{D}$, which can be expressed as

$$\mathbf{D} = \mathbf{UWV^T} \text{ (eq. S1)}$$

where $U = (u_{1, \ldots, u_n})$ is a $2m$ X n matrix forming a set of n basis chemical shift vectors u_i; W is a diagonal matrix whose elements give the singular values sorted in decreasing order; and V is an n X n matrix whose values reflect the proportion of each u_i basis vector from each of the singular values = $(v_1, \ldots, v_n)$. To estimate the non-noise components, we evaluated the singular values and the shapes of the v_i vectors. Large singular value and smooth shape of the v_i vector correspond to a non-noise component (2). In the case of each of the titrations with [^{2}H,^{15}N]-NTF2 and $FSFG_1$, $FSFG_3$, and $FSFG_6$ only the first two components were determined to be non-noise components with the free form of NTF2 as one of the non-noise components.

The non-noise components were used to generate a reconstructed data set, thereby increasing the precision of the affinity analysis for the [^{2}H,^{15}N]-NTF2 titrations. The reduced U ($2m$ X n_c), W (n_c X n_c), and V (n X n_c) matrices from the non-noise components were then used to back-calculate the data matrix D using eq. S1. This resulted in a noise-filtered data set in the form of noise-filtered chemical shift values for each residue. This procedure is analogous to reconstruction using principal component analysis (3).

Discussion on local concentration of FSFG motifs in multivalent interaction

To estimate and to illustrate the change in $[FSFG]_{local}$ as a function of FSFG-FSFG distance, we calculated $[FSFG]_{local}$ for our designed $FSFG_2$ constructs (Figure 1B, right) based on polymer physics theory. Here we defined the $[FSFG]_{local}$ as the concentration of FSFG motifs

within a probing volume defined by the spacer length, *L*. We assumed that the spacer between the two FSFG motifs behaves as a random coil polymer(4) and thus calculated the local concentration based on a three-dimensional random flight model which is equivalent to an ideal chain undergoing random walks (rather than self-avoiding random walks) (5):

$$[FSFG]_{local} = \frac{1}{N_A(\langle r^2\rangle^{\frac{1}{2}})^3}\left(\frac{3}{2\pi}\right)^{\frac{3}{2}} \quad \text{(eq. S2)}$$

where N_A is Avogadro's number and $\langle r^2\rangle^{\frac{1}{2}}$ is the root-mean-square distance (in decimeters) between ends of the spacer

$$\langle r^2\rangle^{\frac{1}{2}} = a\sqrt{n} \quad \text{(eq. S3)}$$

Equation S3 is commonly used in polymer chemistry, where *n* is the number of segments (i.e. amino acids here) that make up the spacer chain, and *a* is related to the distance between two segments. Using distance distribution between adjacent FSFG motifs obtained from our previous simulation (4) as $L = \langle r^2\rangle^{1/2} \approx \langle r\rangle$ = 33.0 Å for adjacent FSFG repeats (*n* = 15), we first calculated *a* to be 8.5 Å. For each construct in the $FSFG_2$ series, we calculated $\langle r^2\rangle^{1/2}$ by multiplying *a* by the number of amino acids separating the two FSFG motifs (eq. S3), and computed the range of $[FSFG]_{local}$ concentrations from Eq. S2 (See Table S3).

The $[FSFG]_{local}$ calculated above is simply the concentration of FSFG motifs that are within the explorable space of the protein. The local concentration effect influences the overall binding reaction by promoting the formation of divalently interacting species (two interaction patches on NTF2 bound by two FSFG motifs on a molecule of $FSFG_2$) or by inducing a rebinding effect (6).

Based on the calculations for variant $FSFG_2$ constructs, we calculated $[FSFG]_{local}$ for $FSFG_3$-$FSFG_{12}$ constructs following the model proposed by Gargano et al. (7) (Table S3). The process is illustrated in Figure S10. First, we calculated and added the individual contribution of each FSFG motif to the overall $[FSFG]_{local}$ in the vicinity of the first binding site for each binding configuration, and then the combinatorial factors for each binding configuration were calculated. Finally, we calculated the average $[FSFG]_{local}$ for each construct using the combinatorial factors as weights for each configuration.

Our estimates of $[FSFG]_{local}$ are consistent in their trends and demonstrate two important points. First, $[FSFG]_{local}$ decreases rapidly as the FSFG-FSFG distance increases for divalent

constructs, suggesting that only the FSFG motifs in the vicinity of the first FSFG motif (that is, engaged to the TF site) contribute significantly to the multivalency effect. This implies that in the NPC where FG motif concentrations are in the millimolar range, distal FG motifs could be easily competed out by bulk FG motifs from another FG Nup molecule, allowing rapid exchange on TF sites. Secondly, the rate of increase in $[FSFG]_{local}$ decreased as the number of FG motifs increased. This is because the additional motifs at the end contribute less to the $[FSFG]_{local}$ as the inter-FG motif distance increases. Consistently, the rate of decrease in K_Ds was also shown to decrease with higher valency.

Simplified kinetic simulations of $FSFG_1$-NTF2 interaction.

We set up simplified kinetic models to illustrate how the difference in K_D values can arise between the forward (fixed $[FSFG_n]$ with varying [NTF2]) and the reverse (fixed [NTF2] with varying $[FSFG_n]$) titrations, using monovalent $FSFG_1$ as an example. The kinetic models used are depicted in Figure S8. Here, we assumed that four FG-interacting sites on an NTF2 molecule and that each site can independently interact with $FSFG_1$ (i.e. no cooperativity) with the same affinity. We ignored any steric effects or sliding between interaction sites (4) for simplicity. We emphasize that the sole purpose of the simplified models discussed here is to illustrate a specific point regarding the origin of differences in K_D values between the forward and reverse titrations and that *they are not equivalent to our exact interpretation of our experimental observations*.

The forward titration was simulated by the model depicted in Figure S8B and described by two differential equations:

$$\frac{d}{dt}S_0 = -4k_{on}[NTF2]S_0 + k_{off}S_1$$

$$\frac{d}{dt}S_1 = 4k_{on}[NTF2]S_0 - k_{off}S_1$$

Likewise, the reverse titration was simulated by the model in Figure S8C and described by the five equations below:

$$\frac{d}{dt}S_0 = -4k_{on}[FSFG_1]S_0 + k_{off}S_1$$

$$\frac{d}{dt}S_1 = 4k_{on}[FSFG_1]S_0 - (3k_{on}[FSFG_1] + k_{off})S_1 + 2k_{off}S_2$$

$$\frac{d}{dt}S_2 = 3k_{on}[FSFG_1]S_1 - (2k_{on}[FSFG_1] + 2k_{off})S_2 + 3k_{off}S_3$$

$$\frac{d}{dt}S_3 = 2k_{on}[FSFG_1]S_2 - (k_{on}[FSFG_1] + 3k_{off})S_3 + 4k_{off}S_4$$

$$\frac{d}{dt}S_4 = k_{on}[FSFG_1]S_3 - 4k_{off}S_4,$$

where k_{on} and k_{off} are on- and off-rate constants, respectively. The numerical constants account for the possible number of permutations to achieve a particular transition. We set $K_{D,\text{mono}}$, the site-to-site dissociation constant (Figure S8A) to 19.9 mM and bound k_{on} and k_{off} by $K_{D,\text{mono}} = k_{off} / k_{on}$. Thus, this $K_{D,\text{mono}}$ defines the intrinsic affinity between a FG motif and one of the four equivalent NTF2 sites in this particular model and remains constant regardless of how the titration is conducted (i.e. this $K_{D,\text{mono}}$ is *not* an apparent one in contrast to the K_D*s* described below) (Fig. S8A). The models were implemented in a matrix form over a range of [NTF2] and [$FSFG_1$] to obtain a complete titration curve. The simulations were run long enough to reach equilibrium so that the result only depended on the ratio of k_{off} to k_{on} (i.e. $K_{D,\ mono}$). The concentration of the titrated protein that saturated half of the *binding sites* (as opposed to molecules) on the other was determined to be the K_D. Thus, in the forward titration, K_D is the [NTF2] that half-saturates the FG motifs in the sample, while in the reverse titration, K_D is the [$FSFG_1$] that half-saturates all the available NTF2 sites. The simulations yielded 4.98 mM K_D for the forward titration and 19.9 mM for the reverse one, demonstrating that the K_D value obtained depends on the number of binding sites and on which species are titrated. We note here that the K_D for the reverse titration is the same as the $K_{D,\text{mono}}$ because the reverse titration tracked the saturation of a single NTF2 site measured in terms of [$FSFG_1$], which is equivalent to the

concentration of FSFG motif due to its monovalency.

We simulated $FSFG_1$ case for simplicity here and the discrepancy in K_Ds between the forward and the reverse titrations can be solely attributed to the number of FG-interacting sites on NTF2. In contrast, the high valency constructs have more complicated interaction mechanisms involving the effect of local concentration and sliding (4).

Dynamic light scattering (DLS)

Dynamic light scattering measurements were made on a Dynapro plate reader (Instruments, Santa Barbara, CA) at 298 K. Experiments were run in a 384 well plate format with independent samples in triplicate. For each sample, 10 acquisitions of 5 s were acquired; and the Dynapro software, DYNAMICS version 7.1.0.25, was used to analyze autocorrelation profiles. The resulting intensity-weighted regularized data was averaged over the triplicate data set and the average radius of hydration was calculated.

Primary sequences of constructs used in this study

$FSFG_1$ (13273.95 Da)

MNETSKPA**FSFG**AKSDEKKDGDASKPASSSGAKPDENKASATSKPASSSGAKPEEKKDDNSS
KPASSSGAKSNEDKQDGTAKPASSSGAKPAEKNNNETSKPASSSGAKSDEKKDGDASKPALE
HHHHHH*

$FSFG_2$ or *FFSSSS* (13394.15 Da)

MNETSKPA**FSFG**AKSDEKKDGDASKPA**FSFG**AKPDENKASATSKPASSSGAKPEEKKDDNSS
KPASSSGAKSNEDKQDGTAKPASSSGAKPAEKNNNETSKPASSSGAKSDEKKDGDASKPALE
HHHHHH*

$FSFG_3$ (13514.34 Da)

MNETSKPA**FSFG**AKSDEKKDGDASKPA**FSFG**AKPDENKASATSKPA**FSFG**AKPEEKKDDNSS
KPASSSGAKSNEDKQDGTAKPASSSGAKPAEKNNNETSKPASSSGAKSDEKKDGDASKPALE
HHHHHH*

$FSFG_4$ (13634.53 Da)

MNETSKPA**FSFG**AKSDEKKDGDASKPA**FSFG**AKPDENKASATSKPA**FSFG**AKPEEKKDDNSS
KPA**FSFG**AKSNEDKQDGTAKPASSSGAKPAEKNNNETSKPASSSGAKSDEKKDGDASKPALE

HHHHHH*

$FSFG_5$ (13754.73 Da)

MNETSKPA**FSFG**AKSDEKKDGDASKPA**FSFG**AKPDENKASATSKPA**FSFG**AKPEEKKDDNSS
KPA**FSFG**AKSNEDKQDGTAKPA**FSFG**AKPAEKNNNETSKPASSSGAKSDEKKDGDASKPALE
HHHHHH*

$FSFG_6$ (13874.92 Da)

MNETSKPA**FSFG**AKSDEKKDGDASKPA**FSFG**AKPDENKASATSKPA**FSFG**AKPEEKKDDNSS
KPA**FSFG**AKSNEDKQDGTAKPA**FSFG**AKPAEKNNNETSKPA**FSFG**AKSDEKKDGDASKPALE
HHHHHH*

$FSFG_{12}$ (25807.75 Da)

MNETSKPA**FSFG**AKSDEKKDGDASKPA**FSFG**AKPDENKASATSKPA**FSFG**AKPEEKKDDNSS
KPA**FSFG**AKSNEDKQDGTAKPA**FSFG**AKPAEKNNNETSKPA**FSFG**AKSDEKKDGDASKPA**FS
FG**AKSDEKKDGDASKPA**FSFG**AKPDENKASATSKPA**FSFG**AKPEEKKDDNSSKPA**FSFG**AKS
NEDKQDGTAKPA**FSFG**AKPAEKNNNETSKPA**FSFG**AKSDEKKDGDASKPALEHHHHHH*

$SSSG_6$ (13153.76 Da)

MNETSKPASSSGAKSDEKKDGDASKPASSSGAKPDENKASATSKPASSSGAKPEEKKDDNSS
KPASSSGAKSNEDKQDGTAKPASSSGAKPAEKNNNETSKPASSSGAKSDEKKDGDASKPALE
HHHHHH*

***FSFSSS* (13273.95 Da)**

MNETSKPA**FSFG**AKSDEKKDGDASKPASSSGAKPDENKASATSKPA**FSFG**AKPEEKKDDNSS
KPASSSGAKSNEDKQDGTAKPASSSGAKPAEKNNNETSKPASSSGAKSDEKKDGDASKPALE
HHHHHH*

***FSSFSS* (13394.15 Da)**

MNETSKPA**FSFG**AKSDEKKDGDASKPASSSGAKPDENKASATSKPASSSGAKPEEKKDDNSS
KPA**FSFG**AKSNEDKQDGTAKPASSSGAKPAEKNNNETSKPASSSGAKSDEKKDGDASKPALE
HHHHHH*

***FSSSSF* (13394.15 Da)**

MNETSKPA**FSFG**AKSDEKKDGDASKPASSSGAKPDENKASATSKPASSSGAKPEEKKDDNSS
KPASSSGAKSNEDKQDGTAKPASSSGAKPAEKNNNETSKPA**FSFG**AKSDEKKDGDASKPALE

HHHHHH*

NTF2 (monomer 15275.86 Da, dimer 30551.72 Da)

MSLDFNTLAQNFTQFYYNQFDTDRSQLGNLYRNESMLTFETSQLQGAKDIVEKLVSLPFQKVQ
HRITTLDAQPASPNGDVLVMITGDLLIDEEQNPQRFSQVFHLIPDGNSYYVFNDIFRLNYSAHHH
HHH*

FSFG single repeat peptide (2127.28 Da)

Aceytl-NETSKPAFSFGAKSDEKKD-NH_2

Supplementary Figures

Figure S1. Titration curves corresponding to fits from NTF2 titration for indicated [^{15}N] FSFG$_n$ constructs.

Chemical shift changes as a function of NTF2 concentration were fit to a shared K_D using Equation 2 for each of the F (blue), S (red), F (green), G (purple) motif residues for each of the FSFG constructs indicated. The remaining titrations appear in Figure 2A.

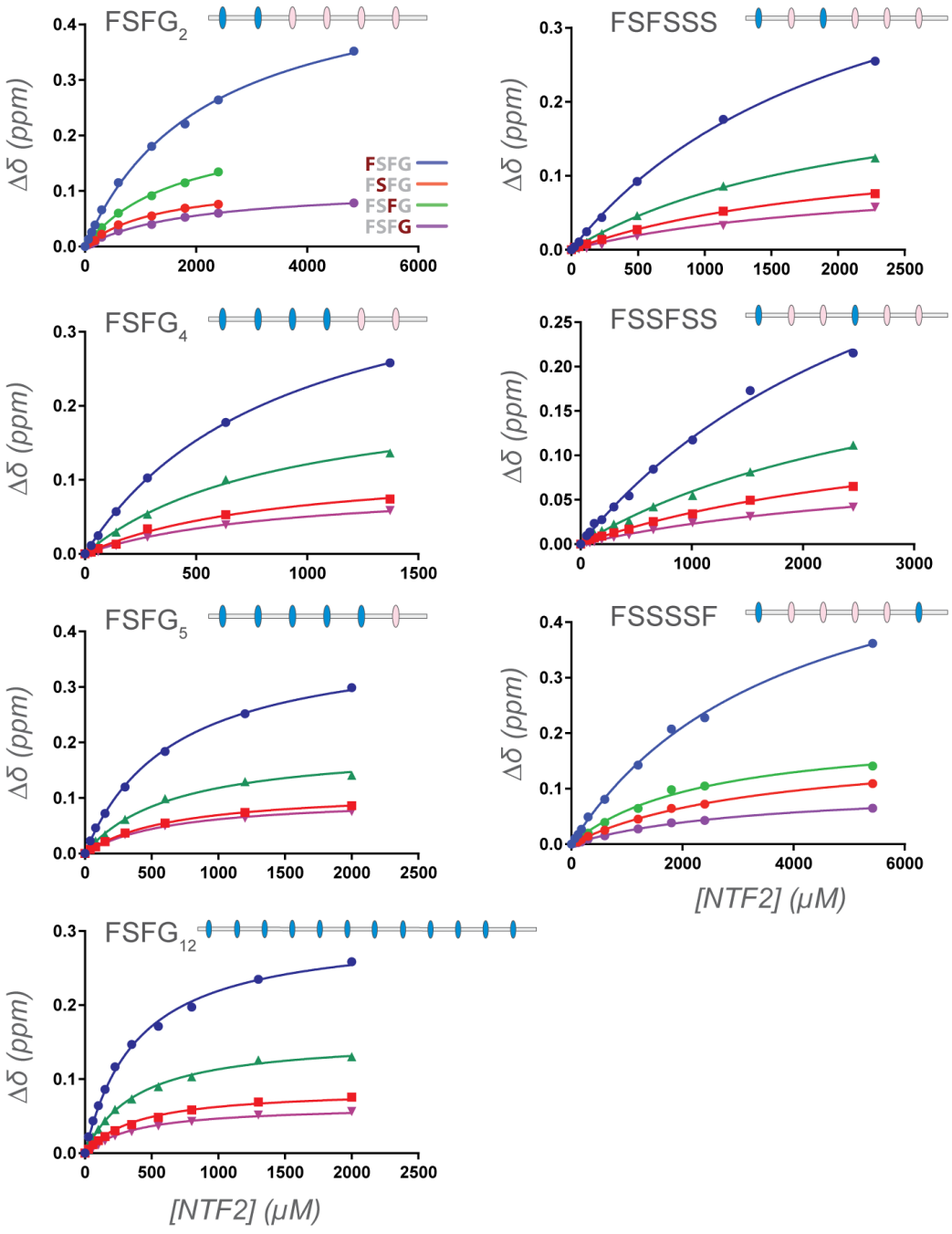

Figure S2. Select ITC measurements for each $FSFG_n$ construct.

Heat evolution of NTF2 titrated with FSFG constructs (top panel), reference-adjusted normalized heat (NDH) curve (bottom, dots) (See Table S2 for experimental conditions), and fitted curve (bottom, red line) for each of the FSFG constructs are indicated.

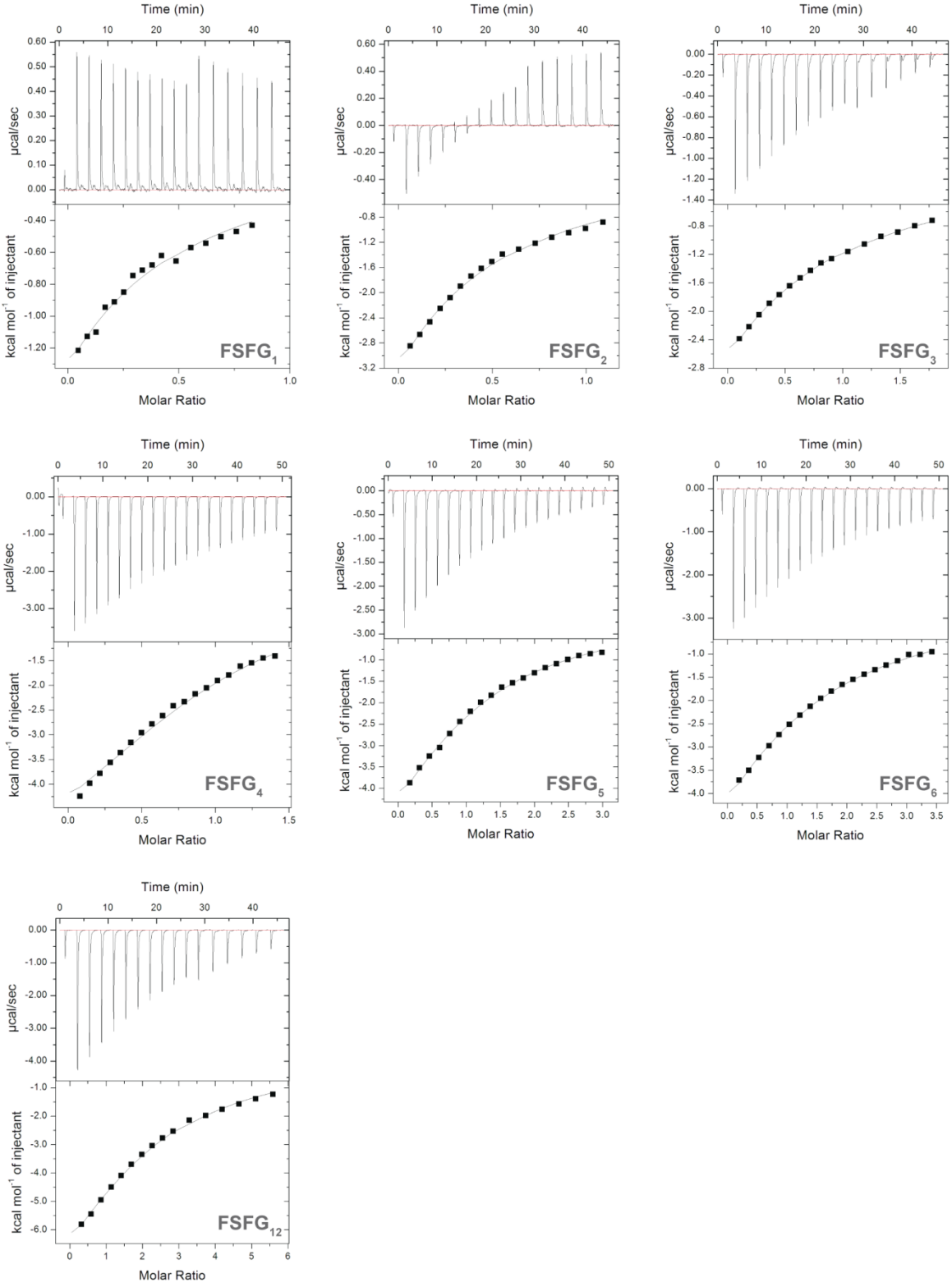

Figure S3. Standard setup of an ITC measurement.

(A) Heat evolution for $FSFG_6$ titrated with NTF2 (A), NTF2 titrated into buffer (B), and buffer titrated into $FSFG_6$ (C), (D) NDH (Normalized heat per injection) curves for each of the heat evolutions (black, $FSFG_6$-NTF2, green, buffer-NTF2, blue, $FSFG_6$-buffer). (E) Reference-adjusted NDH curve for $FSFG_6$ titrated with NTF2 (the green and blue NDH curves were subtracted from the black one in (D) and the fitted curve (red). See experimental procedures for details.

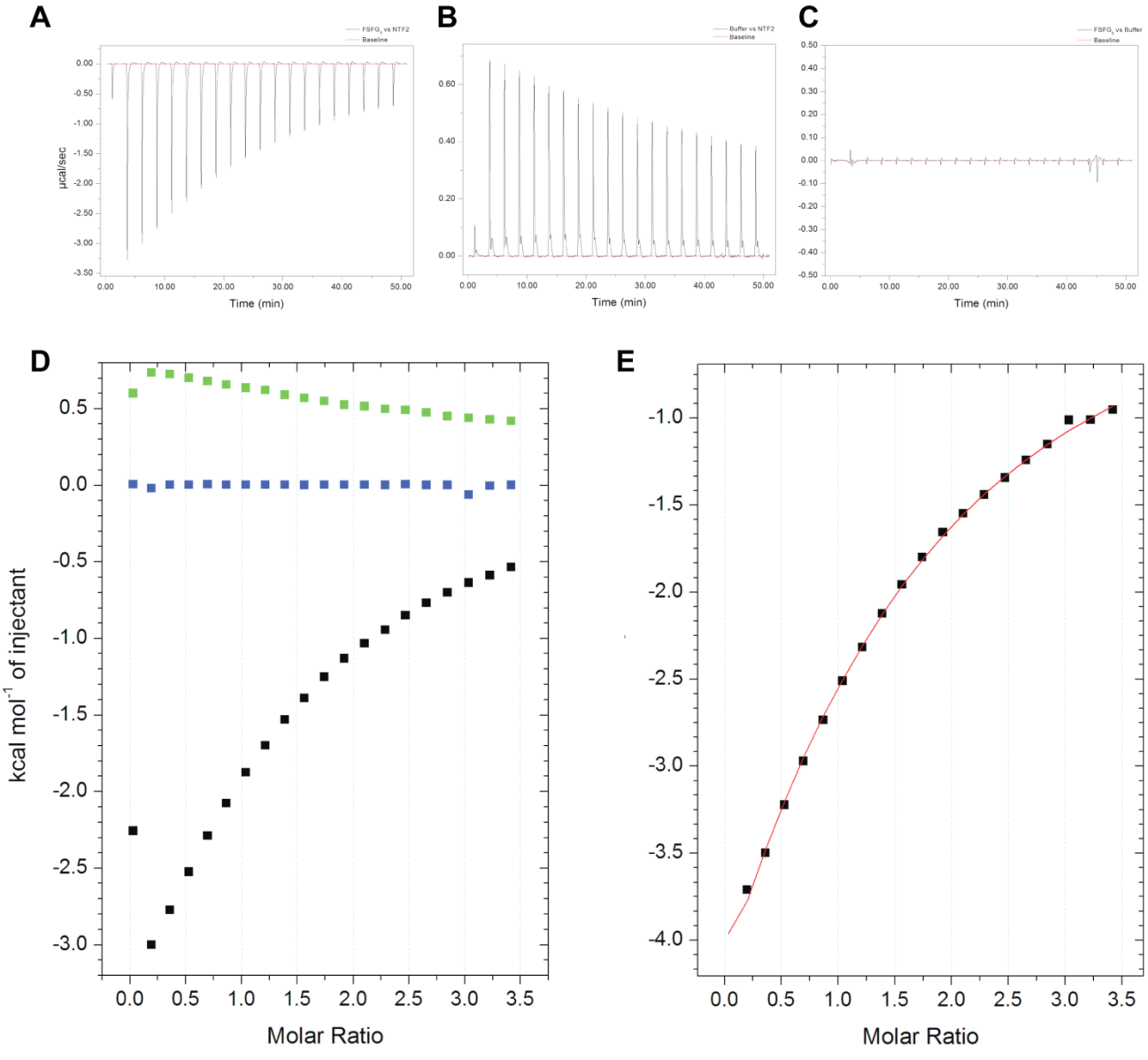

Figure S4. Examples of [^{2}H,^{15}N] NTF2 NMR titration experiments.

TROSY spectra corresponding to NMR titration experiments of (A) 250 μM [^{2}H,^{15}N]-NTF2 with $FSFG_1$, (B) 500μM [^{2}H,^{15}N]-NTF2 with a single repeat FSFG peptide (C) 250μM [^{2}H,^{15}N]-NTF2 with $FSFG_3$ and (D) 500 μM [^{2}H-^{15}N]-NTF2 with $FSFG_6$. The color bar displays the progression of the titration experiment starting from free [^{2}H,^{15}N]-NTF2 (navy blue) to the maximum concentration of FSFG ligand (red). Each titration was performed at 25 °C at 800 MHz. (E) FG-interaction surface on NTF2, shown in a sphere representation, with FSFG peptides, in cyan, displayed at the crystallographic interaction site created based on the chemical shift perturbations observed at the final titration point of [^{2}H-^{15}N]-NTF2 with $FSFG_6$ (PDB: 1GYB (8)). The residues are colored in red if the chemical shift change is greater than half a standard deviation above the mean, in orange, if the chemical shift change is greater than the mean, and in yellow if the chemical shift change is greater than half a standard deviation below the mean.

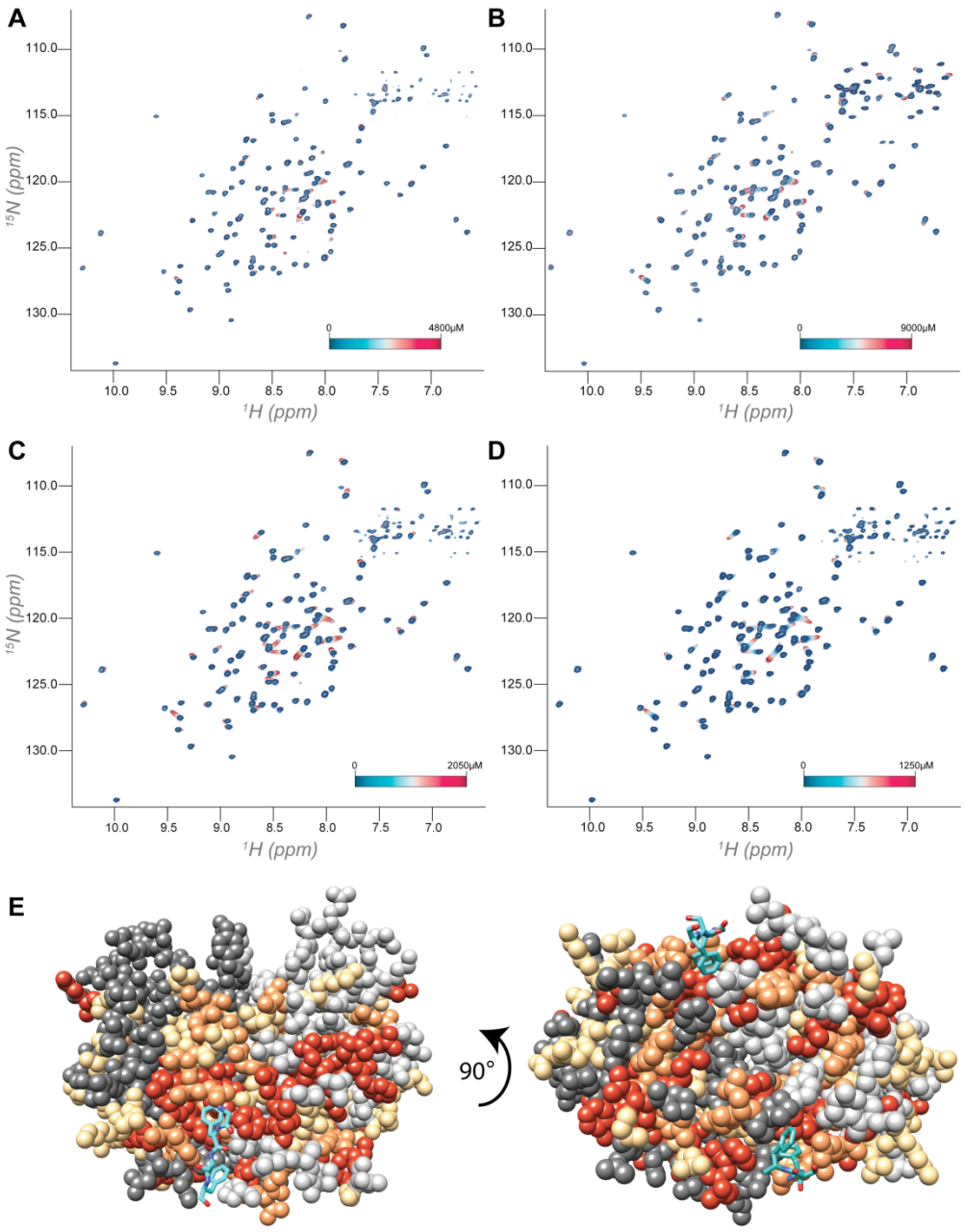
A
B
C
D
E
110.0
115.0
120.0
125.0
130.0
15N (ppm)
10.0
9.5
9.0
8.5
8.0
7.5
7.0
1H (ppm)
0
4800μM
9000μM
2050μM
1250μM
90°

Figure S5. SVD analysis of the titrations of [^{2}H,^{15}N] NTF2 with unlabeled FSFG$_1$, FSFG$_3$, and FSFG$_6$.

The singular values for each component, plotted in decreasing order for (A) FSFG$_1$, (C) the single repeat FSFG peptide, (E) FSFG$_3$, and (G) FSFG$_6$. The shape of the v_i vectors for the first four components plotted versus the number of titration points for (B) FSFG$_1$ and (D) the single repeat FSFG peptide, (F) FSFG$_3$ and (H) FSFG$_6$, respectively. To determine the number of non-noise components, the singular values (A, C, E, and G) must be significantly large and the shape of the v_I vector (B, D, F, and H) must be smooth. Only the first two components in all titrations have smooth shape and large singular values indicating they are non-noise components.

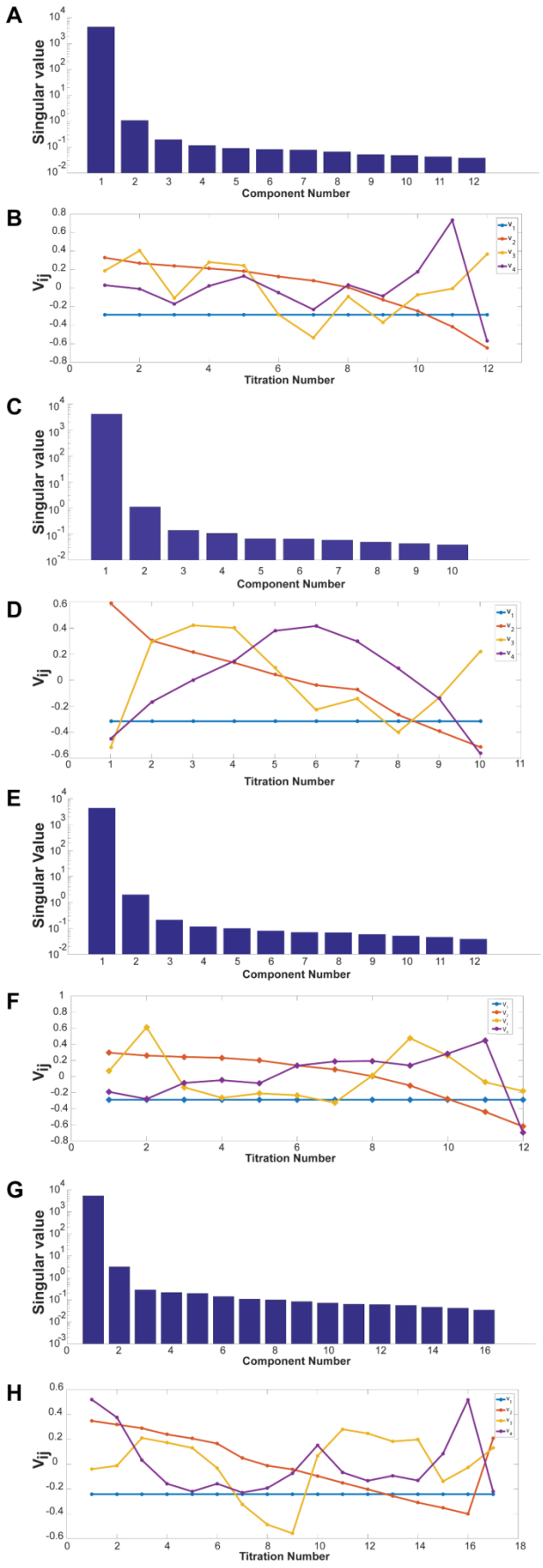

Figure S6. Titration curves resulting from experiments with [^{2}H,^{15}N]-NTF2 and unlabeled $FSFG_n$.

Chemical shift perturbations (CSP) derived from the SVD filtered non-noise dataset were plotted as a function of the concentration of the FSFG construct; (A) $FSFG_1$, (B) a single repeat FSFG peptide, (C) $FSFG_3$, and (D) $FSFG_6$. Each set of titration curves was globally fit to a shared K_D value using Equation 1. Residues were selected if they were showing clear examples of fast-exchange shifts, had CSP larger than the half of a standard deviations below the mean at the titration point with the largest ligand concentration collected and did not yield ambiguous fit results in the local (independent) fit. Under these criteria, 61, 56, 63, and 63 out of 113 assigned NTF2 residues were fitted to Equation 1 for titrations involving $FSFG_1$, a single repeat FSFG peptide, $FSFG_3$, and $FSFG_6$, respectively.

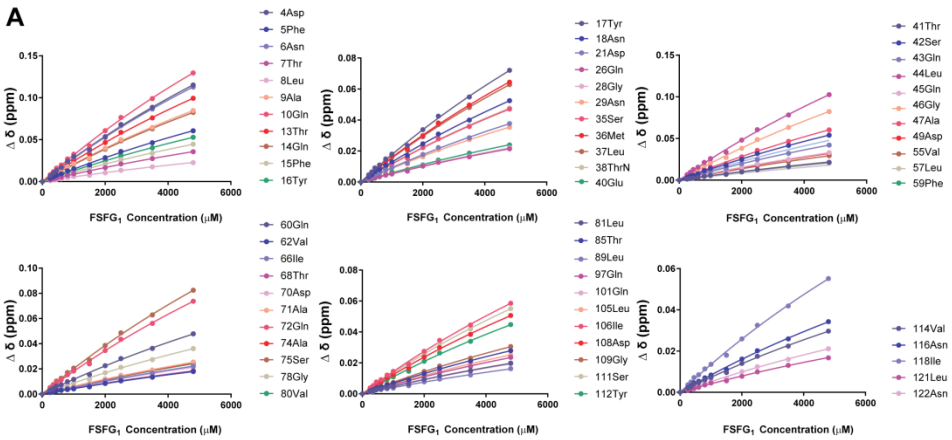
A
Δ δ (ppm)
FSFG1 Concentration (μM)
4Asp
5Phe
6Asn
7Thr
8Leu
9Ala
10Gln
13Thr
14Gln
15Phe
16Tyr
17Tyr
18Asn
21Asp
26Gln
28Gly
29Asn
35Ser
36Met
37Leu
38ThrN
40Glu
41Thr
42Ser
43Gln
44Leu
45Gln
46Gly
47Ala
49Asp
55Val
57Leu
59Phe
60Gln
62Val
66Ile
68Thr
70Asp
71Ala
72Gln
74Ala
75Ser
78Gly
80Val
81Leu
85Thr
89Leu
97Gln
101Gln
105Leu
106Ile
108Asp
109Gly
111Ser
112Tyr
114Val
116Asn
118Ile
121Leu
122Asn

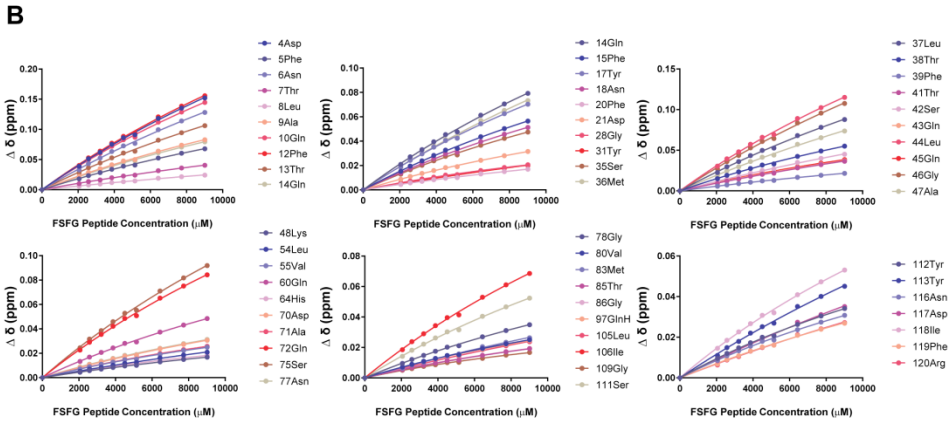
B
Δ δ (ppm)
FSFG Peptide Concentration (μM)
4Asp
5Phe
6Asn
7Thr
8Leu
9Ala
10Gln
12Phe
13Thr
14Gln
14Gln
15Phe
17Tyr
18Asn
20Phe
21Asp
28Gly
31Tyr
35Ser
36Met
37Leu
38Thr
39Phe
41Thr
42Ser
43Gln
44Leu
45Gln
46Gly
47Ala
48Lys
54Leu
55Val
60Gln
64His
70Asp
71Ala
72Gln
75Ser
77Asn
78Gly
80Val
83Met
85Thr
86Gly
97GlnH
105Leu
106Ile
109Gly
111Ser
112Tyr
113Tyr
116Asn
117Asp
118Ile
119Phe
120Arg

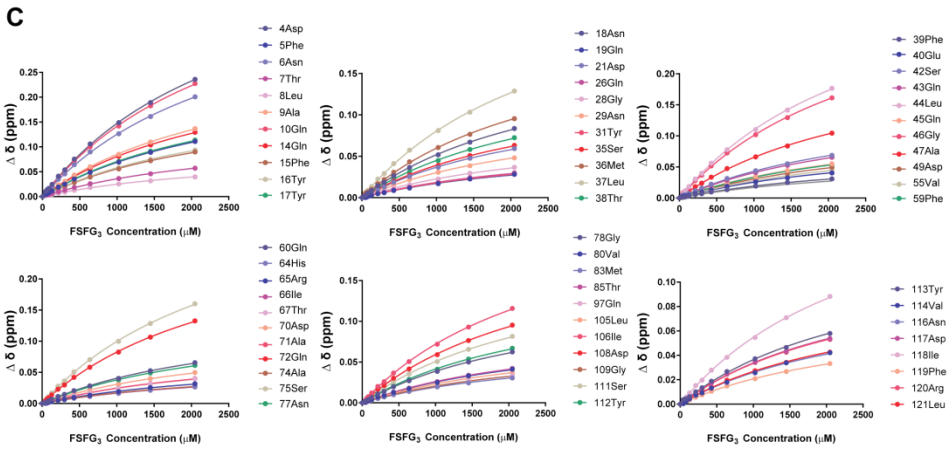
C
Δ δ (ppm)
FSFG3 Concentration (μM)
4Asp
5Phe
6Asn
7Thr
8Leu
9Ala
10Gln
14Gln
15Phe
16Tyr
17Tyr
18Asn
19Gln
21Asp
26Gln
28Gly
29Asn
31Tyr
35Ser
36Met
37Leu
38Thr
39Phe
40Glu
42Ser
43Gln
44Leu
45Gln
46Gly
47Ala
49Asp
55Val
59Phe
60Gln
64His
65Arg
66Ile
67Thr
70Asp
71Ala
72Gln
74Ala
75Ser
77Asn
78Gly
80Val
83Met
85Thr
97Gln
105Leu
106Ile
108Asp
109Gly
111Ser
112Tyr
113Tyr
114Val
116Asn
117Asp
118Ile
119Phe
120Arg
121Leu

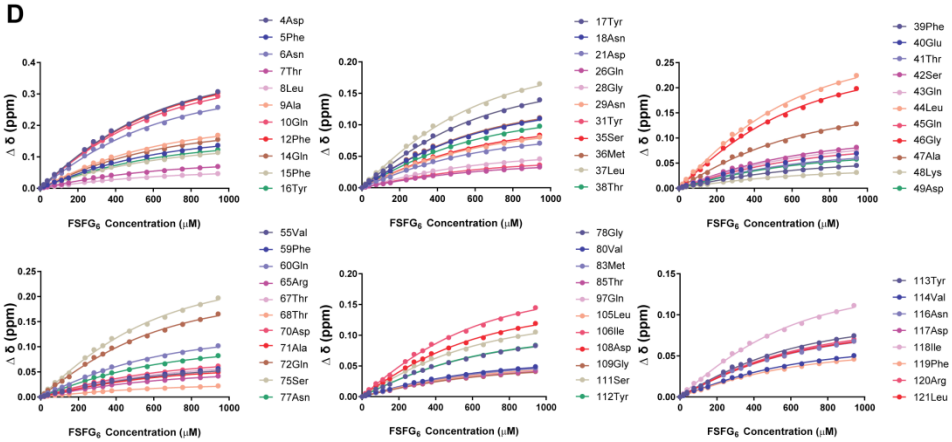
D
Δ δ (ppm)
FSFG6 Concentration (μM)
4Asp
5Phe
6Asn
7Thr
8Leu
9Ala
10Gln
12Phe
14Gln
15Phe
16Tyr
17Tyr
18Asn
21Asp
26Gln
28Gly
29Asn
31Tyr
35Ser
36Met
37Leu
38Thr
39Phe
40Glu
41Thr
42Ser
43Gln
44Leu
45Gln
46Gly
47Ala
48Lys
49Asp
55Val
59Phe
60Gln
65Arg
67Thr
68Thr
70Asp
71Ala
72Gln
75Ser
77Asn
78Gly
80Val
83Met
85Thr
97Gln
105Leu
106Ile
108Asp
109Gly
111Ser
112Tyr
113Tyr
114Val
116Asn
117Asp
118Ile
119Phe
120Arg
121Leu

Figure S7. Derived dissociation constants (K_D) from titrations with [^{2}H,^{15}N] NTF2 and FSFG$_n$ constructs.

Box and whisker plots comparing the determined K_D from local (independent) fitting of either the raw or the SVD non-noise filtered datasets from titrations involving [^{2}H,^{15}N] NTF2 with (A) $FSFG_1$, (B) a single repeat FSFG peptide, (C) $FSFG_3$, and (D) $FSFG_6$. The median, 25th and 75th percentiles and, the minimum, and maximum are shown in box and whisker diagram. As in Fig. S6, 61, 56, 63, and 63 out of 113 assigned residues were fitted to Equation 1 for $FSFG_1$, a single repeat FSFG peptide, $FSFG_3$, and $FSFG_6$, respectively. For $FSFG_1$ fitting with a global K_D value yielded 19.9 ± 0.44* mM and 15.9 ± 1.1 mM for the SVD-filtered and unfiltered datasets, respectively. For the single repeat FSFG peptide, fitting with a global K_D yielded 33.9 ± 0.72* mM and 24.4 ± 1.17 mM for the SVD-filtered and unfiltered datasets, respectively. For $FSFG_3$, fitting with a global K_D yielded 2.41 ± 0.01 mM and 2.29 ± 0.05 mM for the SVD-filtered and unfiltered datasets, respectively. For $FSFG_6$, fitting with a global K_D yielded 0.25 ± 0.01* mM and 0.21 ± 0.01 mM for the SVD-filtered and unfiltered datasets, respectively. (*) indicate whether the K_D best-fit parameter was statistically preferred to be shared compared with independently fit using an extra sum-of-squares F test within GraphPad Prism. The final saturation level achieved was ~19%, ~21%, ~45%, ~70%, for titrations with $FSFG_1$, the single repeat FSFG peptide, $FSFG_3$, and $FSFG_6$ as the titrant, respectively.

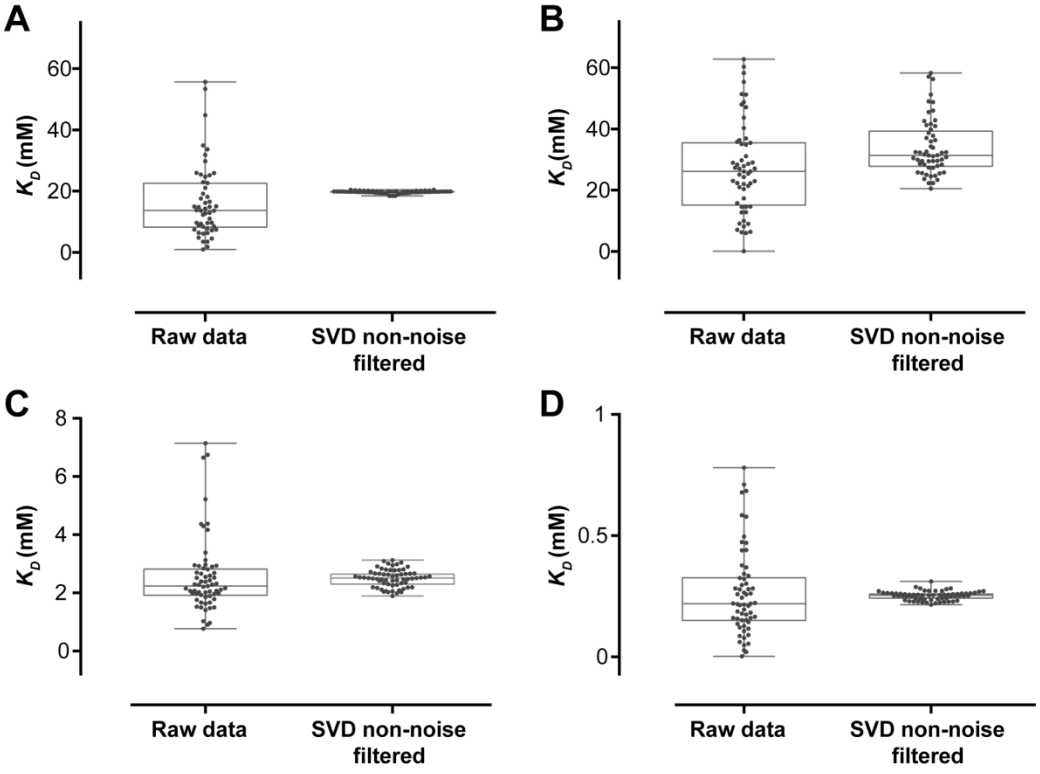

Figure S8. Simulation of $FSFG_1$-NTF2 interaction by simplified kinetic models.

(A) $FSFG_1$ interacting with one of the four identical sites on NTF2. (B) An illustration for the forward titration, with increasing concentration of NTF2. Unbound and bound states were denoted by S_0 and S_1, respectively. (C) An illustration for the reverse titration, with increasing concentration of $FSFG_1$. Unbound, singly bound, doubly bound, triply bound, and quadruply-bound states were denoted by S_0, S_1, S_2, S_3, and S_4, respectively.

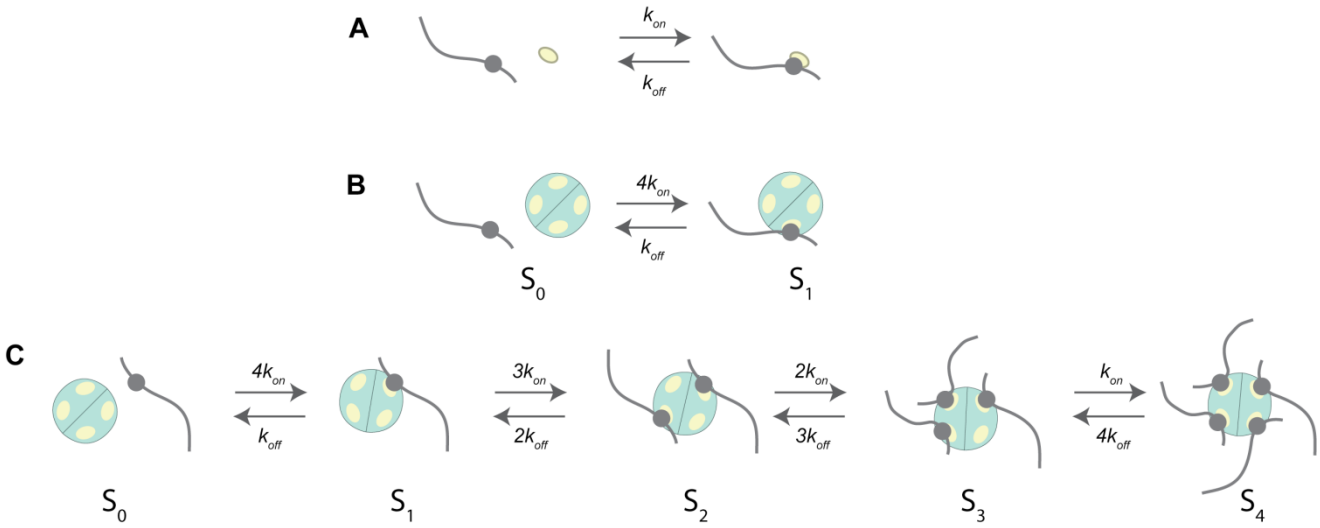

Figure S9. Determination of molecular stoichiometry by dynamic light scattering (DLS). (A) Intensity-weighted DLS of the apo forms of $FSFG_6$, $FSFG_{12}$, and NTF2. (B) Intensity-weighted DLS comparing the apo $FSFG_6$ sample to those in the presence of increasing NTF2 concentrations. For the sample at 1:1 molar ratio, intensity plot is derived from a mixture of free and 1:1 $FSFG_6$:NTF2 molecular stoichiometry. No further increase in the peak position was observed at greater NTF2 concentrations. (C) Intensity-weighted DLS comparing the apo $FSFG_{12}$ sample to those in the presence of increasing NTF2 concentrations. The positions of the peaks in the presence of NTF2 were consistent with a shift from ~1:1 to ~ 2:1 NTF2:$FSFG_{12}$ molecular stoichiometry at higher NTF2 concentrations. (D) Table reporting the radius of hydration, R_h, and the percentage by mass of the peak. In the case of $FSFG_{12}$, two separate peaks could be resolved at 1:5 molar ratio with NTF2, where the smaller of the two likely represent the free protein component. Each measurement represents data averaged from independent samples in triplicate.

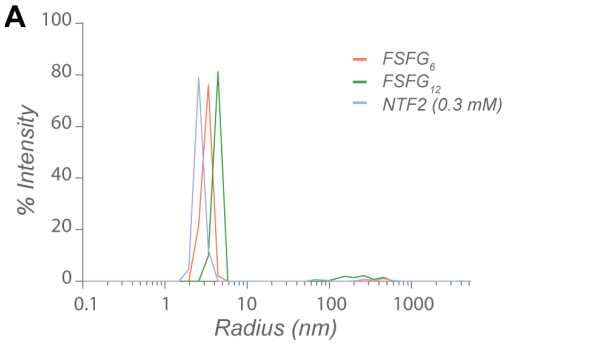

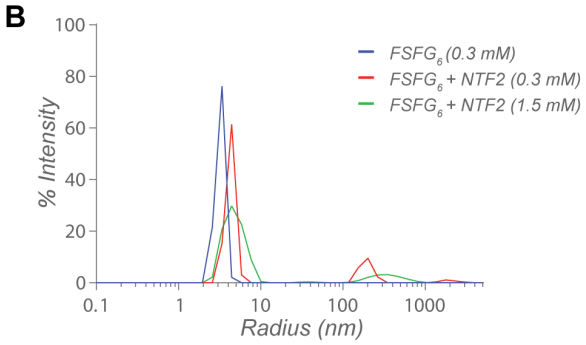

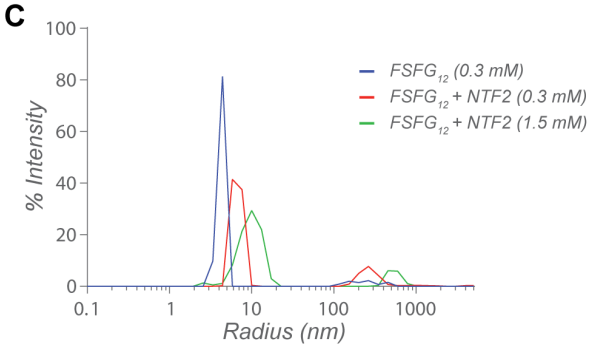

D

Sample	R_h (nm) Peak 1 (% mass)	R_h (nm) Peak 2 (% mass)
NTF2 (0.3 mM)	2.64 (99.99)	–
$FSFG_6$ (0.3 mM)	3.22 (100)	–
$FSFG_6$ + NTF2 (0.3 mM)	4.28 (99.54)	–
$FSFG_6$ + NTF2 (1.5 mM)	4.87 (99.77)	–
$FSFG_{12}$ (0.3 mM)	4.32 (99.89)	–
$FSFG_{12}$ + NTF2 (0.3 mM)	6.70 (98.50)	–
$FSFG_{12}$ + NTF2 (1.5 mM)	3.41 (44.86)	10.10 (53.63)

Figure S10. Schematic diagram on the calculation of local concentrations of FSFG motif for $FSFG_5$ construct.

NTF2 can initially interact with an FSFG motif in three possible binding configurations depicted below. Contribution to the overall $[FSFG]_{local}$ from each FSFG motif is calculated in a distance-dependent manner according to Equations S2 and S3. $[FSFG]_{local}$ for each configuration was calculated as the sum of this individual contribution. The average $[FSFG]_{local}$ was calculated by weighing the $[FSFG]_{local}$ of each configuration proportionally to its combinatorial factor.

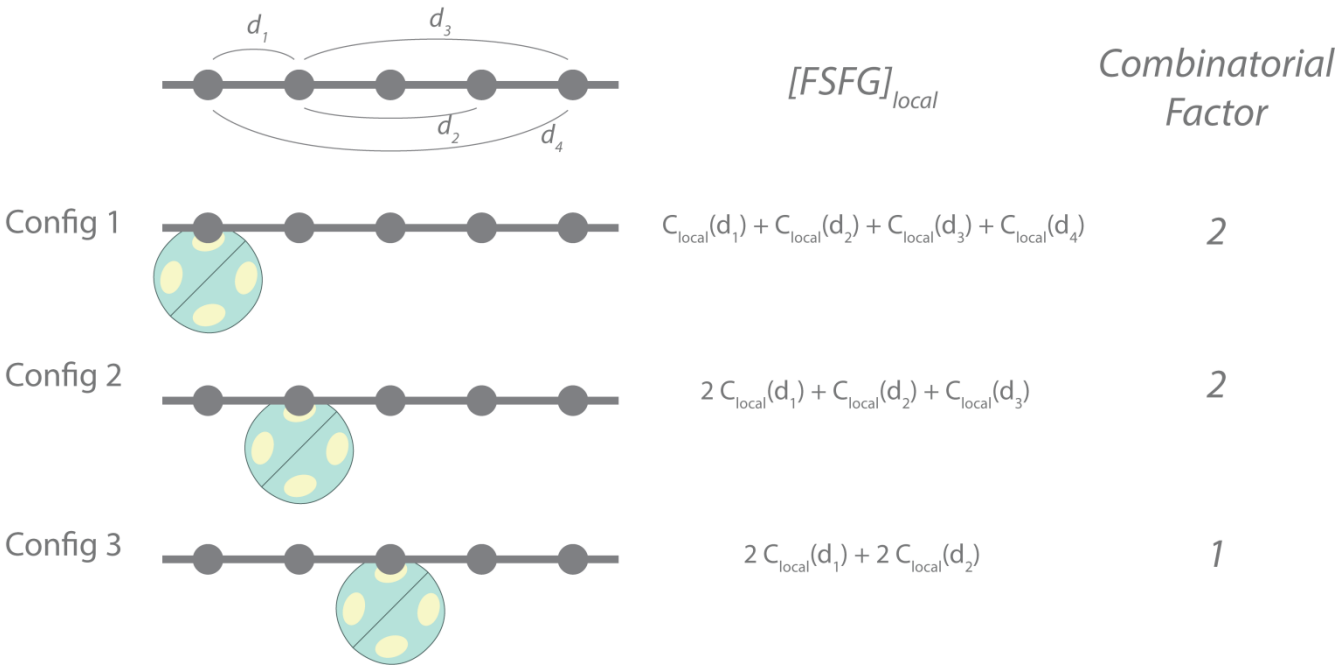

Figure S11. The linear relationship between enthalpy and entropy.

Enthalpy and entropy from each of the individual experiments for $FSFG_4$-$FSFG_{12}$ were plotted (see Table S2 for summary). Dots indicate individual measurements and the plus signs the average measurement for each construct. The linear fit to all the data points yielded a line with a gradient of 0.995 ± 0.02 (RMSE = 0.16, R^2 = 0.995), which were almost identical to the values for the averaged data sets in Fig. 4C (slope = 0.963 ± 0.02, RMSE = 0.05, R^2 = 0.999). The observed linear relationship has a slope near unity, which reflects the small differences in measured ΔG (Table S2) for these constructs.

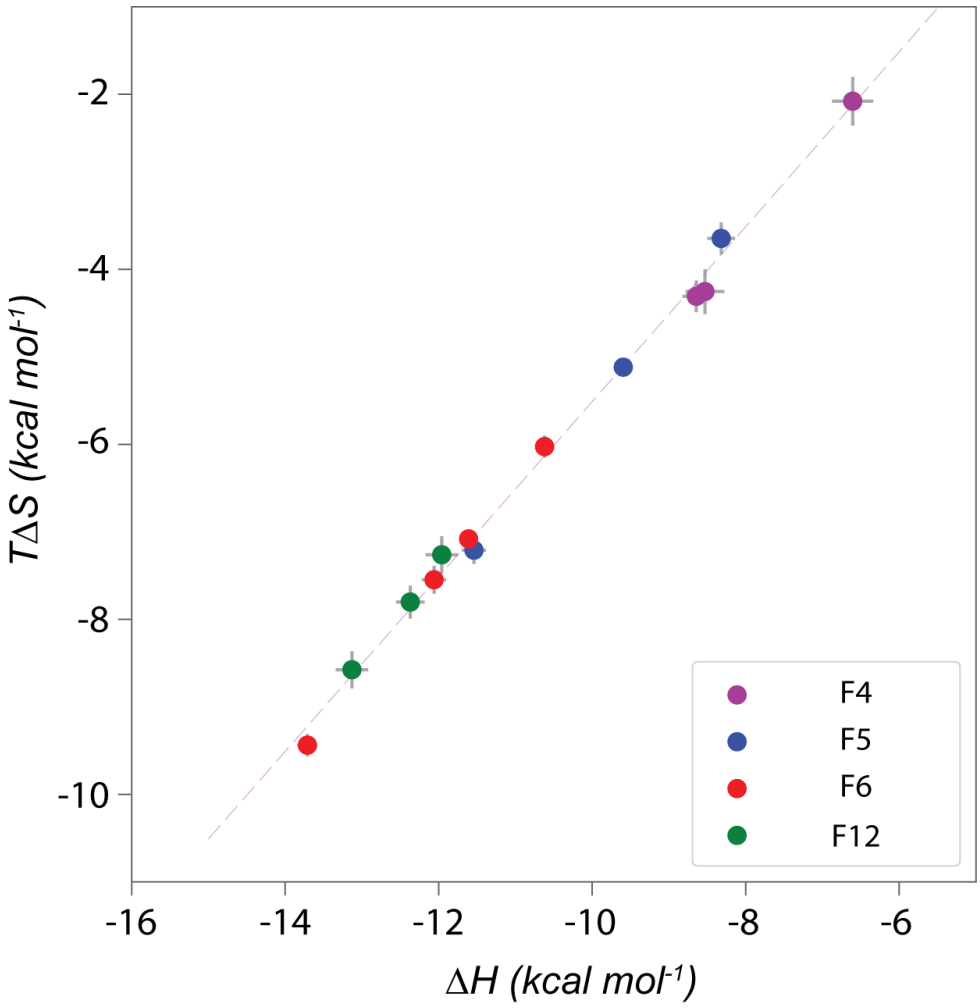

Supplementary Tables

Table S1. Characterization of interaction between FSFG constructs and NTF2

	NMR K_D (mM)	ITC K_D (mM)	ITC ΔG (kcal mol^{-1})	ΔH (kcal mol^{-1})	$-T\Delta S$ (kcal mol^{-1})	n	$n\Delta H$ (kcal mol^{-1})
$FSFG_1$	4.35 ± 0.20	2.73 ± 0.57	-3.52 ± 0.11	*	*	*	-3.3 ± 1.0
$FSFG_2$	2.03 ± 0.07	1.93 ± 0.38	-3.72 ± 0.12	*	*	*	-4.3 ± 0.8
$FSFG_3$	1.19 ± 0.04	1.02 ± 0.18	-4.12 ± 0.10	*	*	*	-5.2 ± 0.5
$FSFG_4$	0.86 ± 0.03	0.62 ± 0.08	-4.38 ± 0.08	-7.9 ± 0.7	3.5 ± 0.7	1.0	-7.9 ± 0.7
$FSFG_5$	0.64 ± 0.02	0.52 ± 0.08	-4.49 ± 0.10	-9.8 ± 0.9	5.3 ± 0.9	1.0	-9.8 ± 0.9
$FSFG_6$	0.56 ± 0.01	0.53 ± 0.07	-4.48 ± 0.07	-12.0 ± 0.6	7.5 ± 0.6	1.0	-12.0 ± 0.6
$FSFG_{12}$	0.37 ± 0.01	0.42 ± 0.03	-4.61 ± 0.05	-12.5 ± 0.3	7.9 ± 0.3	2.0	-25.0 ± 0.7

Table S2. Conditions and fitting results for individual ITC experiments

Construct	*n*	K_A (M^{-1})	ΔH (kcal/mol)	[$FSFG_n$] (mM)	[NTF2] (mM)	*c*-value	Final Saturation (%)
$FSFG_1$	*	259 ± 88	*	2.11	6.12	*	16.5
$FSFG_1$	*	464 ± 195	*	1.69	5.83	*	23.7
$FSFG_1$	*	460 ± 333	*	1.50	6.00	*	24.9
$FSFG_2$	*	746 ± 98	*	2.09	5.89	*	28.1
$FSFG_2$	*	550 ± 158	*	1.25	6.27	*	29.7
$FSFG_2$	*	379 ± 156	*	1.20	6.20	*	23.8
$FSFG_3$	*	800 ± 94	*	0.69	6.12	*	39.7
$FSFG_3$	*	1330 ± 41	*	0.62	5.00	*	45.3
$FSFG_3$	*	1750 ± 150	*	0.69	6.12	*	56
$FSFG_3$	*	569 ± 45	*	0.70	6.00	*	32.4
$FSFG_3$	*	1340 ± 94	*	0.50	6.20	*	52.7
$FSFG_3$	*	957 ± 195	*	0.50	6.20	*	45.2
$FSFG_4$	1.0	1370 ± 86	-8.5 ± 0.25	0.51	6.12	0.70	53
$FSFG_4$	1.0	2090 ± 236	-6.6 ± 0.27	0.82	5.57	1.72	54.9
$FSFG_4$	1.0	1510 ± 66	-8.6 ± 0.18	0.50	6.20	0.76	55.7
$FSFG_5$	1.0	1920 ± 49	-9.6 ± 0.05	0.39	5.57	0.74	59.5
$FSFG_5$	1.0	2670 ± 142	-8.3 ± 0.18	0.40	6.00	1.07	68.2
$FSFG_5$	1.0	1500 ± 42	-11.5 ± 0.16	0.40	6.00	0.60	56.8
$FSFG_6$	1.0	1360 ± 24	-13.7 ± 0.13	0.30	5.00	0.41	49.9
$FSFG_6$	1.0	2040 ± 57	-12.1 ± 0.16	0.30	6.00	0.61	64
$FSFG_6$	1.0	2340 ± 61	-10.6 ± 0.12	0.3	6.20	0.70	67.7
$FSFG_6$	1.0	2100 ± 31	-11.6 ± 0.08	0.3	6.20	0.63	65.4
$FSFG_{12}$	2.0	2790 ± 117	-12 ± 0.21	0.2	3.81	1.12	60.6
$FSFG_{12}$	2.0	2190 ± 80	-13.1 ± 0.21	0.2	5.39	0.88	64.2
$FSFG_{12}$	2.0	2240 ± 87	-12.4 ± 0.19	0.3	6.20	1.34	66.8

[$FSFG_n$] and [NTF2] indicate concentrations of proteins added to the cell and the syringe of the calorimeter, respectively. See the method section for calculation of *c*-values and saturation levels. Asterisks (*) indicate the values could not be reliably estimated from the ITC fitting procedure (see methods).

Table S3. Measured affinity and estimated $[FSFG]_{local}$ for FSFG constructs

Construct	NMR K_D (mM)	$[FSFG]_{local}$ (mM)	Final saturation (%)
$FSFG_2$	2.03 ± 0.07	15.3	70.2
FSFSSS	2.13 ± 0.10	4.5	51.4
FSSFSS	3.27 ± 0.23	2.3	42.6
FSSSSF	3.49 ± 0.18	1.0	60.7
$FSFG_1$	4.35 ± 0.20	-	39.9
$FSFG_3$	1.19 ± 0.04	23.5	80.6
$FSFG_4$	0.86 ± 0.03	28.8	61.2
$FSFG_5$	0.64 ± 0.02	32.5	75.7
$FSFG_6$	0.53 ± 0.01	35.3	78.9

Additional References

1. Turnbull, W. B., and Daranas, A. H. (2003) On the value of c: can low affinity systems be studied by isothermal titration calorimetry? *Journal of the American Chemical Society* **125**, 14859-14866
2. Arai, M., Ferreon, J. C., and Wright, P. E. (2012) Quantitative analysis of multisite protein-ligand interactions by NMR: binding of intrinsically disordered p53 transactivation subdomains with the TAZ2 domain of CBP. *Journal of the American Chemical Society* **134**, 3792-3803
3. Wold, S., Esbensen, K., and Geladi, P. (1987) Principal component analysis. *Chemometrics and intelligent laboratory systems* **2**, 37-52
4. Raveh, B., Karp, J. M., Sparks, S., Dutta, K., Rout, M. P., Sali, A., and Cowburn, D. (2016) Slide-and-exchange mechanism for rapid and selective transport through the nuclear pore complex. *Proceedings of the National Academy of Sciences of the United States of America* **113**, E2489-2497
5. Krishnamurthy, V. M., Semetey, V., Bracher, P. J., Shen, N., and Whitesides, G. M. (2007) Dependence of effective molarity on linker length for an intramolecular protein-ligand system. *Journal of the American Chemical Society* **129**, 1312-1320
6. Weber, M., Bujotzek, A., and Haag, R. (2012) Quantifying the rebinding effect in multivalent chemical ligand-receptor systems. *J Chem Phys* **137**, 054111
7. Gargano, J. M., Ngo, T., Kim, J. Y., Acheson, D. W., and Lees, W. J. (2001) Multivalent inhibition of AB(5) toxins. *Journal of the American Chemical Society* **123**, 12909-12910
8. Bayliss, R., Leung, S. W., Baker, R. P., Quimby, B. B., Corbett, A. H., and Stewart, M. (2002) Structural basis for the interaction between NTF2 and nucleoporin FxFG repeats. *The EMBO journal* **21**, 2843-2853